MARSTRUCT benchmark study on nonlinear FE simulation of an experiment of an indenter impact with a ship side-shell structure

Jonas W. Ringsberg[1,¥], Jörgen Amdahl[2], Bai Qiao Chen[3], Sang-Rai Cho[4], Sören Ehlers[5], Zhiqiang Hu[6], Jan M. Kubiczek[5], Mihkel Kõrgesaar[7], Bin Liu[8], Janis N. Marinatos[9], Karol Niklas[10], Joško Parunov[11], Bruce W.T. Quinton[12], Smiljko Rudan[11], Manolis Samuelides[9], Carlos Guedes Soares[3], Kristjan Tabri[13], Richard Villavicencio[14], Yasuhira Yamada[15], Zhaolong Yu[2], Shengming Zhang[14]

[1] Department of Mechanics and Maritime Sciences, Chalmers University of Technology, Gothenburg, Sweden

[2] Department of Marine Technology/Centre for Autonomous Marine Operations and Systems (AMOS), Norwegian University of Science and Technology, Trondheim, Norway

[3] Centre for Marine Technology and Ocean Engineering (CENTEC), Instituto Superior Técnico, Universidade de Lisboa, Lisbon, Portugal

[4] Department of Ship Building and Marine Engineering, University of Ulsan, Ulsan, Korea

[5] Institute for Ship Structural Design and Analysis, Hamburg University of Technology, Hamburg, Germany

[6] School of Engineering, Newcastle University, Newcastle upon Tyne, UK

[7] Department of Mechanical Engineering, Aalto University, Espoo, Finland

[8] School of Transportation, Wuhan University of Technology, Wuhan, China

[9] Marine Structures Division, School of Naval Architecture and Marine Engineering, National Technical University of Athens, Athens, Greece

[10] Faculty of Ocean Engineering and Ship Technology, Gdansk University of Technology, Gdansk, Poland

[11] Department of Naval Engineering and Marine Technology, University of Zagreb, Zagreb, Croatia

[12] Faculty of Engineering and Applied Science, Memorial University of Newfoundland, St. John's, Newfoundland, Canada

[13] School of Engineering, Department of Civil Engineering and Architecture, Tallinn University of Technology, Tallinn, Estonia

[14] Global Technology Centre, Lloyd's Register EMEA, Southampton, United Kingdom

[15] National Institute of Maritime, Port and Aviation Technology, Tokyo, Japan

[¥] **Corresponding author:**

E-mail: Jonas.Ringsberg@chalmers.se; Tel.: +46-(0)31-7721489

ABSTRACT

This paper presents a benchmark study on collision simulations that was initiated by the MARSTRUCT Virtual Institute. The objective was to compare assumptions, models, modelling techniques and experiences between established researchers within the field. Fifteen research groups world-wide participated in the study. An experiment involving an indenter that penetrates a ship-like side-shell structure was used as the case study. A description of how the experiment was performed, a geometry model of it, and material properties were distributed to the participants prior to their simulations. The paper presents the results obtained from the fifteen FE simulations and the experiment. It presents a comparison of, among other factors, the reaction force versus the indenter displacement, internal energy absorbed by the structure versus the indenter displacement, and analyses of the participants' ability to predict failure modes and events that were observed in the experiment. The outcome of the study is a discussion and recommendations regarding mesh element size, failure criterion and damage models, interpretation of material data and how they are used in a constitutive material model, and finally, uncertainties in general.

Keywords: benchmark study, experiment, failure criteria, failure modes, finite element analysis, ship collision.

Nomenclature

List of abbreviations

DOF	Degrees of Freedom
FE	Finite Element
FEA	Finite Element Analysis
FEM	Finite Element Method

List of symbols

B	Breadth of the test object [m]
E	Elastic modulus [Pa]
H	Height of the test object [m]
K	Hardening coefficient [Pa]
l	Element length in FE model [m]
L	Length of the test object [m]
n	Hardening exponent [-]
t	Element thickness in the FE model [m]

W Width of the test object [m]

x, y, z Coordinates [m]

ε_f Fracture strain [-]

ε_n Necking strain [-]

ε_{true} True strain [-]

σ_{true} True stress [Pa]

σ_y Yield stress [Pa]

1. Introduction

The impact resistance of a ship or offshore structure subjected to collision can be quantified by the energy absorbed by the structure during its deformation and fracture. Explicit finite element (FE) analysis is an established method that is used to simulate collisions and analyse various collision scenarios and the crashworthiness of the structures involved. Recent advancements in computational capacity, resources and commercial FE software have reduced the computation time and made it easier for engineers and researchers to carry out crashworthiness studies of large-scale and complex marine structures. One should, however, not underestimate the challenges involved in ensuring that realistic and reliable results are obtained from these types of simulations and studies, which require in-depth understanding of factors coupled in the simulation model and analysis procedure, for example, choice of element type, mesh resolution, modelling and representation of material characteristics (elastic-plastic deformation, failure criterion, damage modelling, element size, strain-rate effects, etc.), contact conditions, boundary conditions and numerical setting related to the FE software used and its solver.

It is important to continuously strive for model validation to ensure that the results from numerical simulations and predictions can form a solid basis for decision making in, e.g., the design of safe ships. Several investigations in the literature have shown how challenging it is to capture the sequential degradation and failure of a collided structure because of plastic deformation, fracture of its parts (sheets, stiffeners) and collapse by buckling (web frames, stiffeners). Ehlers et al. [1] presented FE simulations of the collision response of three different ship side structures. The study focused on determining the influence of different failure criteria and mesh sensitivity on the force-penetration results. Recommendations for element size and element length to thickness ratio were suggested, together with the failure criteria utilised in the study. Hogström et al. [2] presented an experimental and numerical study of the effects of length scale and strain state on the necking and fracture behaviours in sheet metals. They applied the results reported by Hogström et al. [3] in a parameter

study of the material characteristics' influence on damage stability analyses of a collided ship. Recommendations on how ship collision analyses should be established were proposed, considering, among other factors, the dispersion of the material, failure criterion, modelling of striking bow section, friction and contact conditions, collision angle and striking ship speed.

Ship side and bottom structures are mainly composed of stiffened panels and web girders, whose impact strengths have been investigated extensively [4, 5]. Liu and Guedes Soares [6] and Liu et al. [7] have presented methods that combine external dynamics and internal mechanics in ship collisions for design appraisal assessments. Recently, there has been growing interest in the internal mechanics of structures impacted by a bulbous bow structure. Yu and Amdahl [8] proposed a full 6 DOF coupled simulation procedure for collision and grounding accidents, using an approximation of the hydrodynamic loads that captures the major effects of the fluid. Zhang and Pedersen [9] re-examined the validity and accuracy of the simplified method proposed by Pedersen and Zhang [10] for ship collision damage analysis in ship design assessments by comprehensive validations with experimental results from the public domain. It was concluded that the damaged spaces in heavy collisions can be assumed to be the same as the contour of the penetrated rigid bow of the striking vessel, and the rupture strain of the materials can be taken from standard coupon tensile tests.

Over the past several years, numerical analyses such as finite element analysis (FEA) have been widely used to investigate the structural performance of ships and offshore structures (see, e.g., Paik [11] and Ehlers et al. [12]) because of the development of high-performance computers. However, the definitions of certain parameters in FEA strongly influence the calculated structural load capacity. Kõrgesaar et al. [13] presented ship collision simulations considering four different fracture criteria, three different mesh densities and two different material models in ABAQUS. The failure criterion was also examined by Liu et al. [14] and further examined and extended in [15]. Liu et al. [16] developed a numerical method for simulating structure impact problems and studied the effects of mesh sizes on failure strain and the impact response of a stiffened plate impacted laterally by a spherical indenter using LS-DYNA.

Marinatos and Samuelides [17] presented a numerical method for modelling of the material, i.e., material curve and rupture criterion, considering the effects of mesh size and strain-rate effect on the results. Subsequently, they applied the proposed method in numerical simulations of eighteen indentation tests conducted by different research groups using three different failure criteria. They concluded that realistic simulation of the tests and consistency in terms of the representation of the deformation patterns and the estimation of the absorbed energy is achieved with the criterion based on

the maximum equivalent plastic strain with a cut-off value for triaxialities equal to -1/3, below which the criterion is not activated. The threshold value of strain depends on the element length over thickness ratio, and the authors suggested that close to the area of interest this ratio should be between two and four, i.e., $2 \leq l/t \leq 4$. On that basis, a failure criterion that includes the combined effect of mesh size and stress triaxiality on the failure strain was proposed by Walters [18]. The reasoning behind such a scaling framework is that the effect of mesh size on the FE solution depends on the amount of strain localisation, which varies depending on the stress state [19]. Kõrgesaar and Kujala [20] proved that the approach was feasible based on a comparison with available experimental data, the force-displacement curves of smaller panels and large-scale collision experiments. In addition, the effect of bending on the mesh size sensitivity of the analysis was discussed by Storheim et al. [21].

Experimental work is important to the validation of numerical models, and different efforts have been dedicated relatively recently to configurations that have aspects in common with those studied in this paper [4, 6, 22-24]. Both analytically based methods and finite elements have been used to assess the absorbed energy, but the details of the process can only be described by finite element approaches. Quinton et al. [25] demonstrated experimentally that hull capacity is significantly affected by whether an impact load acts entirely normal to the hull (and thus is stationary with respect to the hull location throughout the entire time history of the impact) or has a tangential component (and thus "slides" or "moves" along the hull during the impact). The authors showed that sliding loads causing plastic damage incite a structural response that varies as low as one-half the response of a similar structure under a stationary load of similar magnitude. That experimental work corroborates similar numerical predictions previously reported by Hong and Amdahl [26]. The present paper addresses the numerical prediction of hull response and onset and the development of hull fracture due to "stationary" impacts. It is important to note that the simulation of stationary loads is a special case of the more general problem of simulating sliding loads. One should not assume that the techniques appropriate for simulating stationary loads are sufficient for predicting responses to sliding loads.

2. Objective, description of benchmark study

Benchmark studies are important in comparing different research groups' skills, best practices, assumptions and "traditions" regarding how to design numerical models and simulate and analyse, e.g., the structural response of a complex ship or offshore structure subjected to an impact load. Even if modelling guidelines and best practices are available, there are always sources of errors and uncertainties that lead to scatter in the simulation results. Benchmark studies help to compare and learn from all participants and systematically identify issues that require improvements and sometimes new

guidelines. Some important questions these studies discuss and try to answer are how large is the scatter in the results that can be accepted, which indicators or criteria should be used in the assessment, and probably most important of all, how can the lessons learnt be communicated to provide improvements and revised best practices.

The objective of this investigation was to present a benchmark study on participants' ability, expertise and recommendations on how to design FE models for collision simulations. A reference experiment in which an indenter penetrates a ship-like structure was used as a case study. The case was designed to be similar to the realistic case in which a striking ship's bulb penetrates the side-shell structure of a struck ship during a collision. Figure 1 presents a schematic and a photograph of the experiment involving the double-hull side-shell structure, which is penetrated by a solid half-sphere. Measurements from th(a)e experiment and stress-strain data from uniaxial tensile tests of the steel material in the structure were made available to the participants through previous work reported by Karlsson et al. [25].

Fig. 1. (a) Geometry of the side-shell structure and the indenter used in the benchmark study and **(b)** a photograph of the experimental setup.

Fifteen research groups world-wide participated. All are active in researching the collision and grounding of ships and offshore structures, and they have published numerous scientific papers on the topic. The majority of the participants are active in both the International Ship and Offshore Structure Committee (ISSC) [28] and in the MARSTRUCT Virtual Institute [29], which coordinated the benchmark study through the lead author of this paper. The participants received the same information, instructions, data and files prior to the start of the study:

- The geometric model of the setup: the side-shell structure, the indenter, and a reinforcing frame for the boundary conditions and control of the failure modes of the structure; see Section 2 for more details.
- The dimensions of all parts of the structure.
- The stress-strain curve obtained from uniaxial tensile tests of the material composing the side-shell structure.
- Coefficients from a curve fit of the stress-strain curve.
- Clear definitions of the boundary conditions.

- Definitions of the contact point and conditions between the indenter and the top of side-shell structure.
- The material properties of the rigid indenter.
- A description of how the experiment was carried out: the displacement-controlled conditions, the load rate and when the experiment was terminated.

The participants submitted individual reports of their results and recommendations on how to design the FE model and perform the numerical simulation of the experiment. The information in these reports was compiled and is presented in this study:

- Detailed description of the FE model and all assumptions that were made, e.g., choice of finite element type and mesh resolution of the different parts of the structure.
- The FE software and version that was used.
- Modelling of the boundary conditions in the experiment.
- Modelling of the contact and loading conditions in the experiment.
- Choice of constitutive material model for simulating the elastic-plastic behaviour of the material, which material data were used in the model, and whether strain-rate effects were considered in the model.
- The choice of failure model/criterion that was used in the FE analysis together with the used and assumed properties.
- Other models and assumptions made, such as Barba's law [30] for the effect of elements' dimensions on the value of the fracture strain.

Three types of results were reported by each participant: (1) the reaction force-indenter displacement curve, (2) the internal energy-indenter displacement curve, and (3) a table presenting the indenter displacement value at which a structural member failed/fractured, buckled, etc. in the FE simulation. These results were compared among the participants and discussed in relation to how the different FE models were designed and the simulations were performed. Section 3 of this paper provides a brief summary of the reference experiment. In Section 4, a summary of the fifteen FE models is presented, followed by a comparison of the results from the FE simulations and the experiment in Section 5. The section includes a discussion of the results and recommendations for how this type of FE simulation should be carried out with respect to the FE model parameters, constitutive material model and failure criteria. The conclusions of the study are presented in Section 6.

3. Reference experiment

The ship-like structure test geometry designed by Karlsson et al. [27] was used as the reference structure. It resembles a typical double-hull side-shell structure (hereafter referred to as the test object) of a ship subjected to a collision load, where the bulb of the striking ship penetrates the struck ship structure. To fit the test object to the testing machine, the object was scaled to one-third the size of a similar full-scale ship structure. This section provides a brief description of the experimental setup and how the experiment was carried out to make the presentation of the benchmark study complete. A detailed description and analyses of the experiment are presented by Hogström et al. [3] and Karlsson et al. [27].

3.1 Description of the test object, boundary and contact conditions

The test object consisted of one outer and one inner side-shell, web/stringer sheets, web/stringer beams and stiffeners in the form of L-profiles. The global dimensions $L \times W \times H$ of the structure were 1500 mm $\times$ 1090 mm $\times$ 300 mm, and the sheet thickness was between 3 mm for the thinnest elements and 5 mm for the thickest structural elements. To establish well-defined boundary conditions, a reinforcing rigid frame was designed around the structure. Figure 2 shows the geometry and the dimensions without the reinforcing frame.

Fig. 2. Dimensions of the test object, from Karlsson et al. [27].

The reinforcing frame was designed and welded around the test object along its edges to create clamped boundary conditions and to ensure well-controlled failure modes of the structure. The lower part of the frame was welded to a rigid fixture. Four displacement transducers were positioned in two directions on the supporting frame and fixture. The transducers measured the frame's deformations to ensure that the fixture's deformations during the tests were negligible; see Fig. 3 for the experimental setup, where two of the displacement transducers are shown in front and to the left of the test object.

Fig. 3. Photograph of the test object in the test rig with the indenter (half-sphere), the reinforcing frame welded to the rigid fixture, and the displacement transducers.

The test object was manufactured from K240-Z shipbuilding mild steel. The indenter was created as a solid (rigid) half-sphere with a radius of 135 mm and made from SS2541 steel. Friction tests without lubrication were carried out by Karlsson et al. [27], who showed that the kinematic friction coefficient was 0.23±0.01 for the current contact conditions.

3.2 Test procedure and measurements

The test object was mounted in a press machine with a 20 MN load capacity. To relax the residual stresses caused by welding the test object's sheets to the frame before the test, the indenter was pushed perpendicularly to load and unload the structure at low speed ten times. The magnitude of the load in this loading sequence was within the elastic region of the material.

The indenter penetrated the structure with a constant displacement rate of 4 mm/s. The collision point was located at the centre of the sheet (see Fig. 3), and the loading direction was perpendicular to the upper sheet's surface. The experiment was interrupted when the lower sheet was fully penetrated by the indenter. Throughout the experiment, the resultant force in the load cell, the position of the indenter, and the displacement transducers on the rigid frame were monitored and recorded. The total calculated measurement uncertainty for the maximum force was less than 1%. The reported uncertainty corresponded to an approximately 95% confidence interval around the measured value; see Karlsson et al. [27] for details.

4. Finite element models and analyses of the experiment

The participants of the benchmark study created their FE models by using the geometry file that defined the geometries of the test object, the indenter and the reinforcing frame. None of the welds were modelled in the FE models. The indenter was modelled as a rigid body and was allowed to move only in the direction perpendicular to the upper sheet at a constant displacement rate. Figure 4 shows an example of an FE model with and without the reinforcing frame; the rigid indenter is not shown in the figure. Table 1 presents a summary of the participants' different FE model definitions and parameters. Two FE solvers were used, ABAQUS [31] and LS-DYNA [32]; all modelling details referring to these solvers can be found in the corresponding references.

Fig. 4. Example of an FE model of the test object:
(a) with the reinforcing frame and **(b)** without the reinforcing frame.

Table 1. Summary of the participants' FE model definitions and parameters.

The majority of the participants carried out convergence analyses to determine the mesh size of the FE model. All participants used four-node shell elements with five section points through the thickness. "Element size" in Table 1 refers the primary size of the elements in the parts of the structure that undergo failure and fracture under the numerical simulation. Recommended practice prescribes that

the element length to thickness ratio, l/t, should be approximately 5. It should be noted that l/t varies from 2 to 6 among the FE models in Table 1.

The users of ABAQUS/Explicit used the "general contact conditions" criterion to define the contact conditions together with the coefficient of frictions presented in Table 1. This contact criterion enforces contact constraints using a penalty contact method, which searches for node-into-face and edge-into-edge penetrations. Similarly, the users of LS-DYNA used the coefficient of frictions in Table 1 but two different contact criteria: "automatic surface-to-surface" for the contact between the indenter and the test object and "automatic single surface" for the contacts between other structural components. Furthermore, it should be noted that to save computation time, the indenter speeds were often much higher in the FE analyses compared with those in the physical experiment, without, however, exhibiting any dynamic effects. The material properties did not include any effects from high loading rates; further details are provided in this section.

The indenter was assumed to be rigid with a Young's modulus of 206 GPa, Poisson's ratio of 0.3 and density of 7,850 kg/m^3. The test object and reinforcing frame were originally manufactured from K240-Z shipbuilding mild steel with a density of 7,850 kg/m^3 and Poisson's ratio 0.3. The properties of this material were determined based on a few tensile tests carried out and presented by Karlsson et al. [27]. The results were, however, not sufficient for detailed modelling and calibration of material parameters for different types of failure and fracture criteria. Therefore, Hogström et al. [3] carried out an in-depth investigation of material properties and parameters for the K240-Z shipbuilding mild steel and the similar NVA shipbuilding mild steel for which additional test results were available and more tests were carried out. It was found that the K240-Z and NVA shipbuilding steels had similar properties. Hence, the latter was used in the current study because more material parameters could be provided to the participants of the benchmark study.

Figure 5 presents the stress-strain curve obtained from uniaxial tensile tests of the NVA shipbuilding mild steel. The participants received the raw data from the experiment. The isotropic hardening of the inelastic stress-strain relation follows the power law described by Eq. (1). The values of the material parameters that describe the non-linear material behaviour were calculated by curve fitting and shared with the participants: yield stress, σ_y = 290 MPa; hardening coefficient, K = 616 MPa; hardening exponent, n = 0.21; necking strain, ε_n = 21%; and fracture strain, ε_f = 26%; the Young's modulus was 206 GPa.

$$\sigma_{true} = K(\varepsilon_{true})^n \quad (1)$$

Fig. 5. True stress-strain relationship for the NVA shipbuilding mild steel.

Table 2 presents a summary of the constitutive material models and their parameters for each FE model. In all of the cases, the material was represented by a nonlinear elastic-plastic constitutive material model with isotropic hardening. Because the physical experiment was carried out at low speed, strain-rate effects were considered negligible, i.e., they were disregarded in the analyses. The summary shows that the participants used the provided information in different ways, using more than the two possibilities that were suggested; they implemented either the raw data from the uniaxial tensile test or the material properties that can be used in the power law for isotropic hardening of the inelastic stress-strain.

Table 2. Constitutive material models and material parameters for the test object and the reinforcing frame.

One large difference between the FE models was related to which failure criterion was preferred and how the damage was modelled. The majority of the participants used a failure criterion that does not consider stiffness degradation after the necking point. Few participants used a multiple damage criterion that separates the damage and failure processes into damage initiation (from the strain at the yield stress to the strain at the necking point) and damage evolution (from the strain at the necking point to the strain at the fracture point) and thereby accounts for stiffness degradation after the necking point according to constitutive mechanics principles. Table 3 presents a summary of the failure criteria and the damage models that were used in the FE models. All participants checked or corrected the element size's effect on the value of the fracture strain. It was stated in the comments whether Barba's law [30] or any other model was implemented in the FE model to allow for the fracture strain's dependence on the element size and thickness in different parts of the FE model.

Table 3. Summary of the preferred failure criterion for each FE model, how damage was modelled and values of relevant and used material parameters.

5. Results and discussion

The results of the FE simulations of the reference experiment are presented, compared and discussed with respect to the resultant vertical force versus indenter displacement (Section 5.1), the internal energy versus indenter displacement (Section 5.2), and analyses of deformations and failure modes (Section 5.3), and a general discussion is provided (Section 5.4). As in the experiment, the FE simulations were run until an indenter displacement of 0.5 m was reached. This indenter displacement corresponds to a full penetration of the indenter through both sheets of the test object. It should be noted that the registered signals from the four displacement transducers showed that the reinforcing frame was perfectly rigid throughout the experiment.

5.1 Resultant vertical force versus indenter displacement

Figure 6 shows the resultant vertical force of the indenter versus its vertical displacement. The origin for the measurement of the displacement was on the upper surface of the upper sheet of the structure. The penetration of the upper sheet is depicted by the first peak and the penetration of the lower sheet by the second peak; see Section 5.3 for a detailed analysis of the deformations and failure modes. Overall, the results from the FE simulations capture the trend and show good agreement with the experiment. There is minor scatter between the FE simulations, and the result obtained from the experiment is in the middle of all the curves, at least until the intender displacement is approximately 0.35 m. Beyond that value, the majority of the FE simulations overestimate the force at the second peak, where the penetration of the lower sheet occurs, and a small offset in the displacement arises when it occurs. The results in Fig. 6(b) show that neither the users of the FE solver ABAQUS nor those of LS-DYNA mimic the results from the experiment better than the other.

Fig. 6. Resultant vertical force versus displacement of the indenter. **(a)** Results from the reference experiment in [27] and the FE simulations of the benchmark study; **(b)** the same results presented in (a), where the black curves represent the users of the FE solver ABAQUS and the red curves represent the users of LS-DYNA.

5.2 Internal energy versus indenter displacement

The processes of plastic deformation and fracture of the test object are complex. In the design and analysis of crashworthiness of structures, the internal energy, i.e., the energy absorbed through deformation and fracture of the structure, is an important property in resisting external loadings. Figure 7 presents the internal energy versus the displacement of the indenter from the experiment and the FE simulations. Curves No. 2, 3, 7, 9 and 14 show excellent agreement with the curve from the experiment,

and curve No. 8 stands out because it is the only FE simulation that overestimates the internal energy. All other curves underestimate the internal energy relative to that determined by the experiment. The results in Fig. 7(b) show that neither the users of the FE solver ABAQUS nor those of LS-DYNA mimic the results from the experiment better than the other.

Fig. 7. (a) Energy absorbed by the structure versus indenter displacement and **(b)** the same result presented in (a), where the black curves represent the users of the FE solver ABAQUS and the red curves represent the users of LS-DYNA.

5.3 Analysis of deformations and failure modes

Events referring to the deformation and fracture of the test object were identified to enable a comparison between the experiment and the FE models. Table 4 presents the nine events and their indenter displacements, which could easily be identified in an FE simulation but only in eight of the cases in the experiment (event 1 could not be observed). Figure 8 presents markers of the events in the curve from the experiment for the resultant vertical force versus indenter displacement. The markers refer to the mean values of the indenter displacement from FE simulations and the observations and registered values in the experiment. Figure 9 presents snapshots from an FE simulation of the deformed structure for each event.

Table 4. Summary of the preferred failure criterion for each FE model, how damage was modelled and values of relevant and used material parameters.

Fig. 8. Presentation of the events in the curve from the experiment for the resultant vertical force versus indenter displacement. The markers "o" refer to the mean values of the indenter displacement from the FE simulations, and "*" represents the observations in the experiment. The error bars represent the standard deviation for each event from the FE simulations; see Table 4.

Fig. 9. (a) Event 1: initiation of plasticity expansion of the T-beam. **(b)** Event 2: tripping of the T-beam. **(c)** Event 3: buckling of the webs of the two central L-profiles attached to the upper sheet. **(d)** Event 4: fracture initiation of the upper sheet. **(e)** Event 5: folding of the webs of the two central L-profiles attached to the upper sheet. **(f)** Event 6: T-beam off. **(g)** Event 7: T-beam starts to contact with the L-profile attached to the lower sheet. **(h)** Event 8: contact of the indenter with the lower sheet. **(i)** Event 9: fracture initiation of the lower sheet.

The results show rather good agreement between the simulations and the experiment for all the events, except for event 9. Prior to this event, the test object has undergone large plastic deformation and fracture of several structural members. It is a true challenge to capture the last event of the fracture of the lower plate. It is also possible that the predictions made by the FE simulations are within the range of the total uncertainty of the experiment, particularly at the instant that event 9 occurs. Because the results from only one experiment were available, it was not possible to find a better explanation for this deviation.

Not all of the events were observed by all participants of the benchmark study; events 2, 3, 5, 6 and 7 were not identified by everyone. One FE model could not observe any of these 5 events, one FE model missed events 3 and 6, and two other FE models missed event 3. Analyses of the FE models showed that the mesh resolution of the structural members (not the upper and lower sheets) and supporting structures that were involved in the deformation processes leading to these events may not be adequate. Hence, finer meshes of the FE models should have been used.

5.4 Discussion

The summaries of the FE models in Tables 1 to 3 show that the FE models have many similarities but also differences as a result of the variety of assumptions, experiences and interpretations among the participants according to their own best practice. Nevertheless, the total scatter is low, and the agreement with the results from the experiment was found to be generally very good.

Out of the fifteen participants, four used the FE software ABAQUS and eleven used LS-DYNA. The results presented in Figs. 6(b) and 7(b) show that neither the ABAQUS nor LS-DYNA users mimic the results from the experiment better than the other. The results from participants No. 2, 3, 7, 9, 10 and 14 show the best agreement with the experiment with respect to (i) the reaction force versus intender displacement (see Fig. 6), (ii) energy versus indenter displacement (see Fig. 7), and (iii) prediction of the failure modes in Table 4. A model uncertainty analysis of how these FE models were defined showed the following:

- All included the reinforcing frame in the FE model.
- They used a mesh size of either 10 or 15 mm, and the fracture strain was adjusted according to Barba's law [30] or the researchers' own methodology.
- Two used ABAQUS but with different failure criteria and damage models; three used LS-DYNA and the same failure criterion.

- All but participant No. 7 used the power law coefficient K and exponent n provided at the outset of the benchmark study; No. 7 used the curve (raw data) from the uniaxial test and created their own curve fit, which can also be observed in the values of the yield stress and the fracture strain (which were included in addition to the mesh size dependence in the method that was used).

The difference between ABAQUS FE models No. 2 and 3 lay in which failure criterion and damage model were used, but this difference caused only a minor variation in the results. Similarly, the difference between LS-DYNA FE models No. 10 and 14 was the mesh size with the adjusted value of the fracture strain; the difference in the Young's modulus was assumed to be negligible for the current case because of the large plastic deformations and fracture processes. The conclusion is that despite these deviations in these factors, they were not sufficient to significantly influence the uncertainty in the prediction of the experiment's characteristics using these FE models.

The force-deformation curves are predicted generally quite well, as expected. Certain differences, however, can be observed, which could be due to the use of different mesh sizes but are more likely due to differences in the adopted stress-strain relationships. It is observed that No. 8 and 13 obtain a high initial peak; this result is expected because they assume a large fracture strain. Model No. 7, on the other hand, which used the largest fracture strain of all, does not follow this trend although the same fracture criterion is used (effective plastic strain). This difference is likely due to a different stress-strain relationship; the early softening and significant deviation from the experimental curve might be explained by early localisation due to less pronounced strain hardening. The use of a high yield stress could also be an indicator. Thus, the force level is good, while the strain level is not as good.

Based on the results of this benchmark study, the authors found it difficult to pinpoint which model parameters or factors contributed the most to the uncertainty in the prediction. The scatter in the results was low, and the participants were observed to have good experience in designing FE models and establishing this type of simulation. It could be a coincidence of small variations in the model definitions that caused five of the FE models to show somewhat less agreement with the reference experiment. In contrast to the FE models 2, 3, 7, 9, 10 and 14,

- No. 1 and 4 used different power law data for K and n, and No. 4 used a different constitutive material model.

- No. 5 did not consider the reinforcing frame in the FE model. Participant and FE model No. 13 did not include the frame either, but other differences in model parameters may have cancelled the effect of not including the reinforcing frame.
- No. 11 used different power law data for K and n and the BWH instability criterion in [21], which did not consider post-necking damage.
- No. 15 featured a different combination of element size and fracture strain compared with the other FE models but essentially had the same other model definitions.

The results from this benchmark study can serve as a guideline on how to design FE models and establish a numerical simulation of ship collisions. The summaries presented in Tables 1 to 3, together with the results discussed in Section 5, show how different combinations, selections and variations of, e.g., element size, failure criterion and damage models, material data and parameters in general affect and contribute to the variability and uncertainty in a numerical simulation of ship collisions. It is strongly recommended to conduct parameter sensitivity analyses prior to "sharp" FE simulations. All the participants of this benchmark study worked according to this principle before they submitted their recommended FE model, its definitions, and simulation results.

6. Conclusions

This paper presented a benchmark study on collision simulations initiated and organised by the MARSTRUCT Virtual Institute. A comparison of the participants' ability, expertise and recommendations on how to perform the explicit FE simulation of an experiment in which an indenter penetrates a ship-like structure was presented. The experiment was designed to be similar to a realistic case in which a striking ship's bulb penetrates the side-shell structure of a struck ship during a collision. Fifteen experienced research groups within the field of ship collision and grounding participated world-wide. The results from fifteen FE models and simulations of the experiment were compared with respect to resultant force versus indenter displacement, internal energy versus indenter displacement, and failure modes of the ship-like structure.

The summary of the results from all FE simulations showed low scatter, and the agreement with the results from the experiment was generally very good. Despite some variations in the FE models regarding, e.g., element size, boundary conditions, constitutive material model and material data used, the differences in the results must be considered acceptable considering the complexity in simulating this type of experiment with large plastic deformation and a number of sequential failure modes of the structure. Regardless of the choice of failure criterion and damage models used in the FE models –

shear failure criterion, equivalent plastic strain criterion, the BWH criterion, a multiple damage criterion with initiation and evolution – the scatter in the results between the FE simulations was acceptable and low. While the majority of the simulations somewhat underestimated the internal energy during the damage process, such an outcome is still considered to be on the "safe side" when considering the safety of the structure.

The main contribution of the study is its intention to serve as a guideline on how to design FE models and establish a numerical simulation of a ship collision. The summaries of the fifteen FE models and the results of their simulations show how different combinations, selections and variations of, e.g., element size, failure criterion and damage models, material data and parameters in general, affect and contribute to the variability and uncertainty in a numerical simulation of ship collisions. It is strongly recommended to conduct parameter sensitivity analyses prior to "sharp" FE simulations. All the participants of this benchmark study worked according to this principle before they submitted their recommended FE model, its definitions, and simulation results.

Acknowledgements

Professor Parunov and Professor Smiljko acknowledge the Croatian Science Foundation under the project 8658 for funding. Dr Niklas is grateful for the financial support from the NCBiR (MARTECII/SmartPS/4/2016) and CI TASK. The contribution from Zijie Song at the Shanghai Jiao Tong University in Shanghai, China, is appreciated very much by Professor Hu. Professor Amdahl and Dr Yu acknowledge the support from the Research Council of Norway, Project AMOS (project no. 223254).

References

[1] Ehlers S, Broekhuijsen J, Alsos HS, Biehl F, Tabri K. Simulating the collision response of ship side structures: a failure criteria benchmark study. International Shipbuilding Progress 2008; 55(1): 127-144.

[2] Hogström P, Ringsberg JW, Johnson E. An experimental and numerical study of the effects of length scale and strain state on the necking and fracture behaviours in sheet metals. International Journal of Impact Engineering 2009; 36(1): 1194-1203.

[3] Hogström P, Ringsberg JW. An extensive study of a ship's survivability after collision – a parameter study of material characteristics, non-linear FEA and damage stability analyses. Marine Structures 2012; 27(1): 1-28.

[4] Villavicencio R, Liu B, Guedes Soares C. Experimental and numerical analysis of a tanker side panel laterally punched by a knife edge indenter. Marine Structures 2014; 37(1): 173-202.

[5] Liu B, Guedes Soares C. Experimental and numerical analysis of the crushing behaviour of stiffened web girders. International Journal of Impact Engineering 2016; 88(1): 22-38.

[6] Liu B, Guedes Soares C. Assessment of the strength of double-hull tanker side structures in minor ship collisions. Engineering Structures 2016; 120(1): 1-12.

[7] Liu B, Villavicencio R, Zhang S, Guedes Soares C. Assessment of external dynamics and internal mechanics in ship collisions. Ocean Engineering 2017; 141(1): 326-336.

[8] Yu Z, Amdahl J. Full six degrees of freedom coupled dynamic simulation of ship collision and grounding accidents. Marine Structures 2016; 47(1): 1-22.

[9] Zhang S, Pedersen PT. A method for ship collision damage and energy absorption analysis and its validation. Ships and Offshore Structures 2017; 12(S1): S11-S20.

[10] Pedersen PT, Zhang S. Absorbed energy in ship collisions and grounding – revising Minorsky's empirical method. Journal of Ship Research 2000; 44(2): 140-154.

[11] Paik JK. Practical techniques for finite element model-ling to simulate structural crashworthiness in ship collisions and grounding (Part II: Verification). Ships and Offshore Structures 2007; 2(1): 81-85.

[12] Ehlers S, Tabri K, Romanoff J, Varsta P. Numerical and experimental investigation on the collision resistance of the X-core structure. Ships and Offshore Structures 2012; 7(1): 21-29.

[13] Kõrgesaar M, Tabri K, Naar H, Reinhold E. Ship collision simulations using different fracture criteria and mesh size. Proceedings of the 33rd International Conference on Ocean, Offshore and Arctic Engineering (OMAE2014), San Francisco, California, USA, 2014. 8-13 June 2014. (OMAE2014-23576)

[14] Liu B, Villavicencio R, Guedes Soares C. On the failure criterion of aluminum and steel plates subjected to low-velocity impact by a spherical indenter. International Journal of Mechanical Sciences 2014; 80(1): 1-15.

[15] Liu B, Villavicencio R, Zhang S, Guedes Soares C. A simple criterion to evaluate the rupture of materials in ship collision simulations. Marine Structures 2017; 54(1): 92-111.

[16] Liu K, Wang Z, Tang W, Zhang Y, Wang G. Experimental and numerical analysis of laterally impacted stiffened plates considering the effect of strain rate. Ocean Engineering 2015; 99(1): 44-54.

[17] Marinatos JN, Samuelides M. Towards a unified methodology for the simulation of rupture in collision and grounding of ships. Marine Structures 2015; 42(1): 1-32.

[18] Walters CL. Framework for adjusting for both stress triaxiality and mesh size effect for failure of metals in shell structures. International Journal of Crashworthiness 2014; 19(1): 1-12.

[19] Kõrgesaar M, Remes H, Romanoff J. Size dependent response of large shell elements under in-plane tensile loading. International Journal of Solids and Structures 2014; 51(21-22): 3752-3761.

[20] Kõrgesaar M, Kujala P. Experimental validation of failure criterion for large complex shell structures. (Editors: S-R Cho, HK Shin, JC, R-T Jung) Proceedings of the 7th International Conference of Collision and Grounding of Ships and Offshore Structures (ICCGS2016), Ulsan, Korea. 15-18 June 2016, pp. 47-53.

[21] Storheim M, Alsos HS, Hopperstad OS, Amdahl J. A damage-based failure model for coarsely meshed shell structures. International Journal of Impact Engineering 2015; 83(1): 59-75.

[22] Villavicencio R, Kim Y-H, Cho S-R, Guedes Soares C. Deformation process of web girders inside of a small-scale laterally impacted tanker double hull structure. Marine Structures 2013; 32(1): 84-112.

[23] Liu B, Villavicencio R, Guedes Soares C. Simplified analytical method to evaluate tanker side panels during minor collision incidents. International Journal of Impact Engineering 2015; 78(1): 20-33.

[24] Liu B, Villavicencio R, Guedes Soares C. Simplified method for quasi-static collision assessment of a damaged tanker side panel. Marine Structures 2015; 40(1): 267-288.

[25] Quinton BWT, Daley CG, Gagnon RE, Colbourne, DB. Experimental investigation of accidental sliding loads on the response of hull plating. (Editors: C Guedes Soares, Y Garbatov) Progress in the Analysis and Design of Marine Structures - Proceedings of the 6th International Conference on Marine Structures (MARSTRUCT2017), Lisbon, Portugal, 8-10 May 2017, pp. 513-522.

[26] Hong L, Amdahl J. Rapid assessment of ship grounding over large contact surfaces. Ships and Offshore Structures 2012; 7(1): 5-19.

[27] Karlsson U, Ringsberg JW, Johnson E, Hosseini M, Ulfvarson U. Experimental and numerical investigation of bulb impact with a ship side-shell structure. Marine Technology 2009; 46(1): 16-26.

[28] MARSTRUCT Virtual Institute. http://www.marstruct-vi.com; 2017 [accessed 9 October 2017].

[29] ISSC2018. International Ship and Offshore Structures Committee 2018, http://www.issc2018.org; 2017 [accessed 9 October 2017].

[30] Davis JR. Tensile testing. Tensile testing. 2nd edition. Materials Park, Ohio: ASM International; 2004.

[31] Dassault Systèmes. ABAQUS software, https://www.3ds.com/products-services/simulia/products/abaqus/; 2017 [accessed 9 October 2017].

[32] Livermore Software Technology Corporation. LS-DYNA software, http://www.lstc.com/products/ls-dyna; 2017 [accessed 9 October 2017].

[33] Swift HW. Plastic instability under plane stress. Journal of the Mechanics and Physics of Solids 1952; 1(1): 1-18.

[34] Cho S-R, Choi S-I, Son S-K. Dynamic material properties of marine steels under impact loadings. Proceedings of the 2015 World Congress on Advances in Structural Engineering and Mechanics (ASEM15), Incheon, Korea. 25-29 August 2015.

[35] Holloman JH. Tensile deformation. Transactions of the Metallurgical Society of AIME 1945; 162(1): 268-290.

[36] Kõrgesaar M, Romanoff J. Influence of mesh size, stress triaxiality and damage induced softening on ductile fracture of large-scale shell structures. Marine Structures 2014; 38(1): 1-17.

[37] Cho S-R, Song S-U, Park S-H, Shin HK. Plastic and fracture damages of double hull structures under lateral collisions. (Editors: C Guedes Soares, Y Garbatov) Progress in the Analysis and Design of Marine Structures - Proceedings of the 6th International Conference on Marine Structures (MARSTRUCT2017), Lisbon, Portugal, 8-10 May 2017, pp. 431-438.

[38] Ehlers S. A procedure to optimize ship side structures for crashworthiness. Proceedings of the Institution of Mechanical Engineers, Part M: Journal of Engineering for the Maritime Environment 2010; 224(1): 1-11.

[39] Alsos HS, Hopperstad OS, Törnqvist R, Amdahl J. Analytical and numerical analysis of sheet metal instability using a stress based criterion. International Journal of Solids and Structures 2008; 45(7-8): 2042-2055.

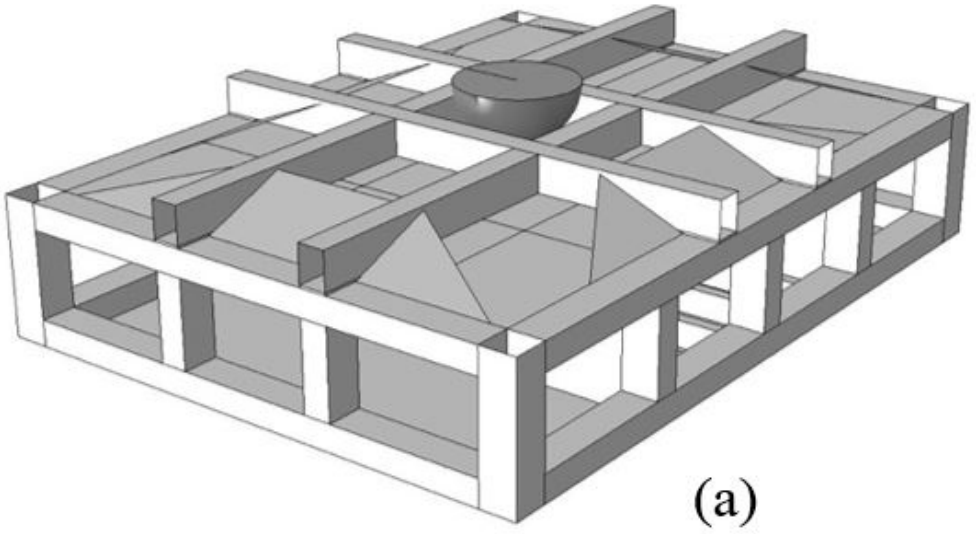

(a)

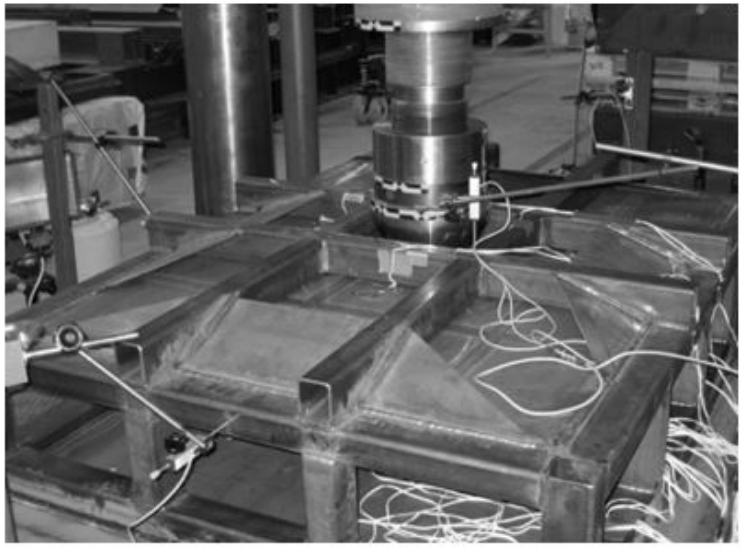

(b)

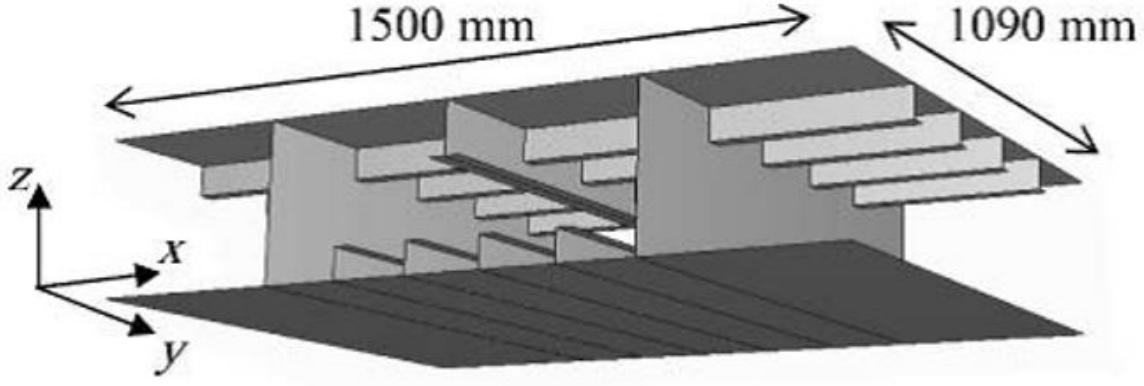

Thicknesses
Upper and lower plate: 5 mm
Vertical plates: 3 mm
L-profiles: 4 mm
T-beam, web: 3 mm
T-beam, flange: 5 mm

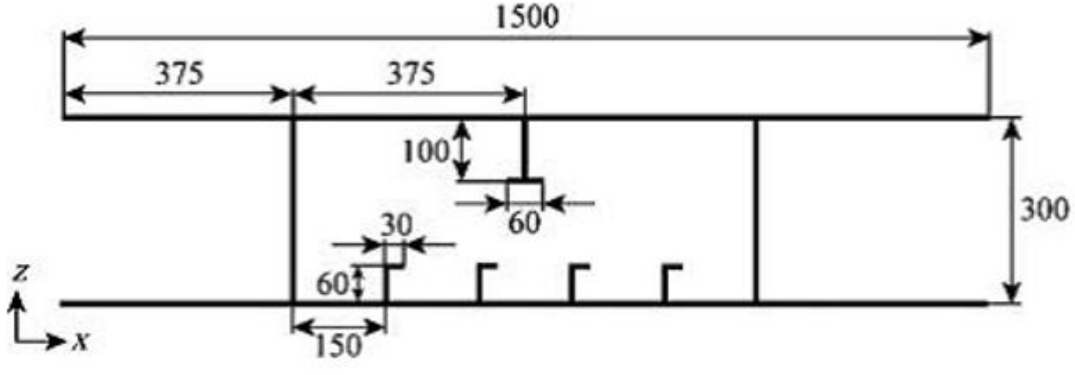

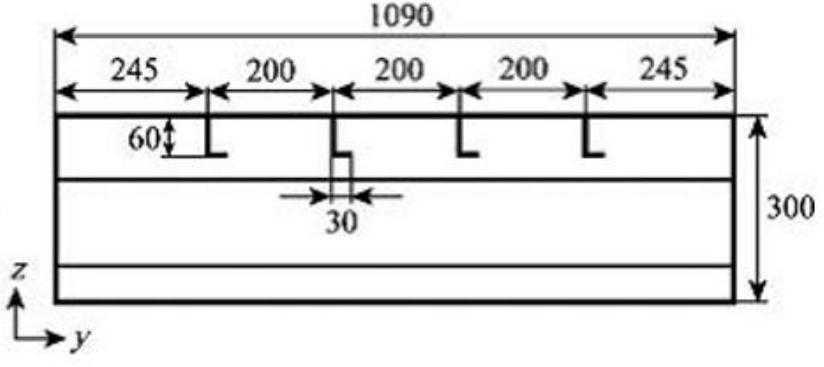

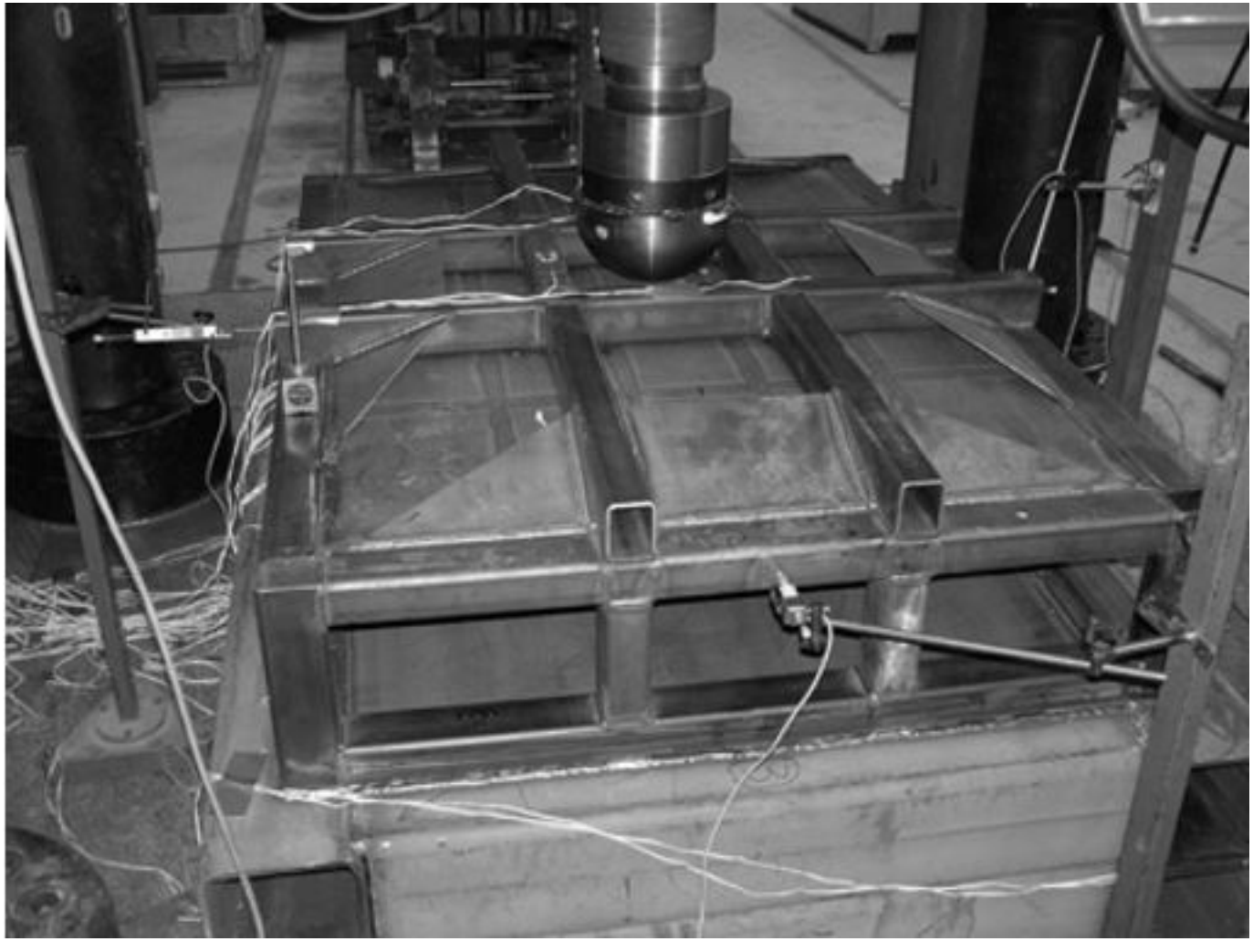

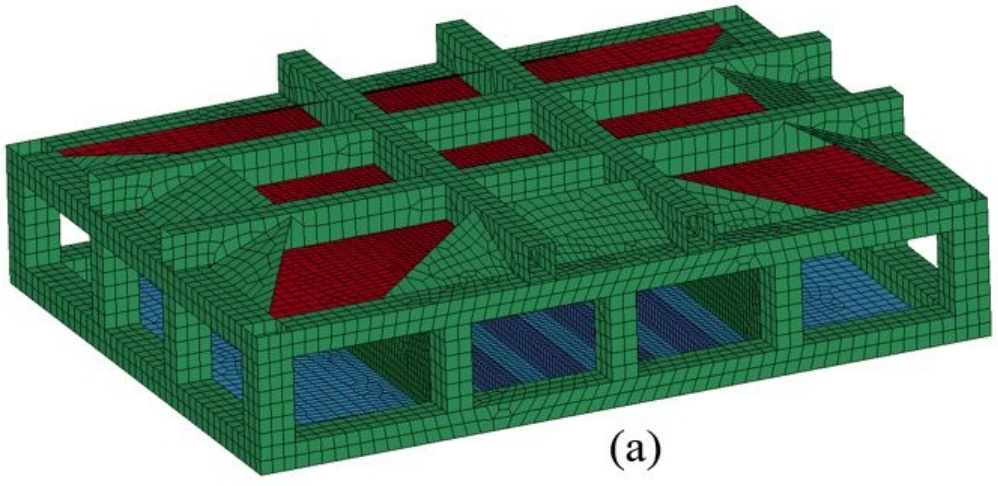

(a)

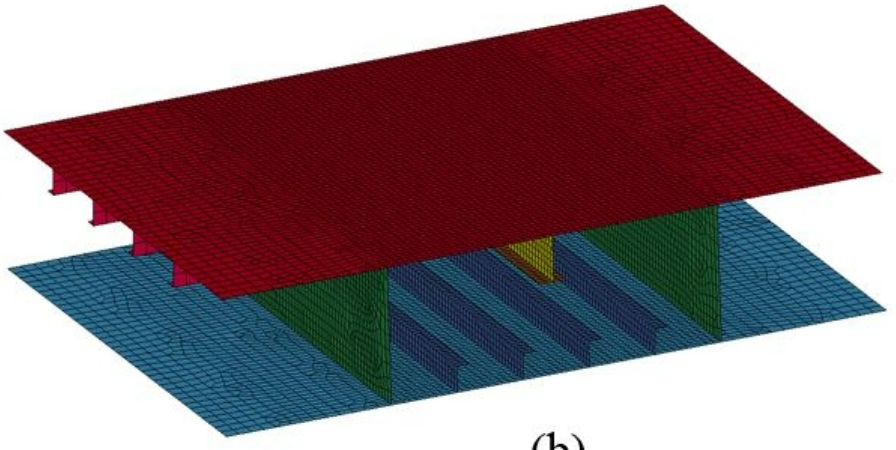

(b)

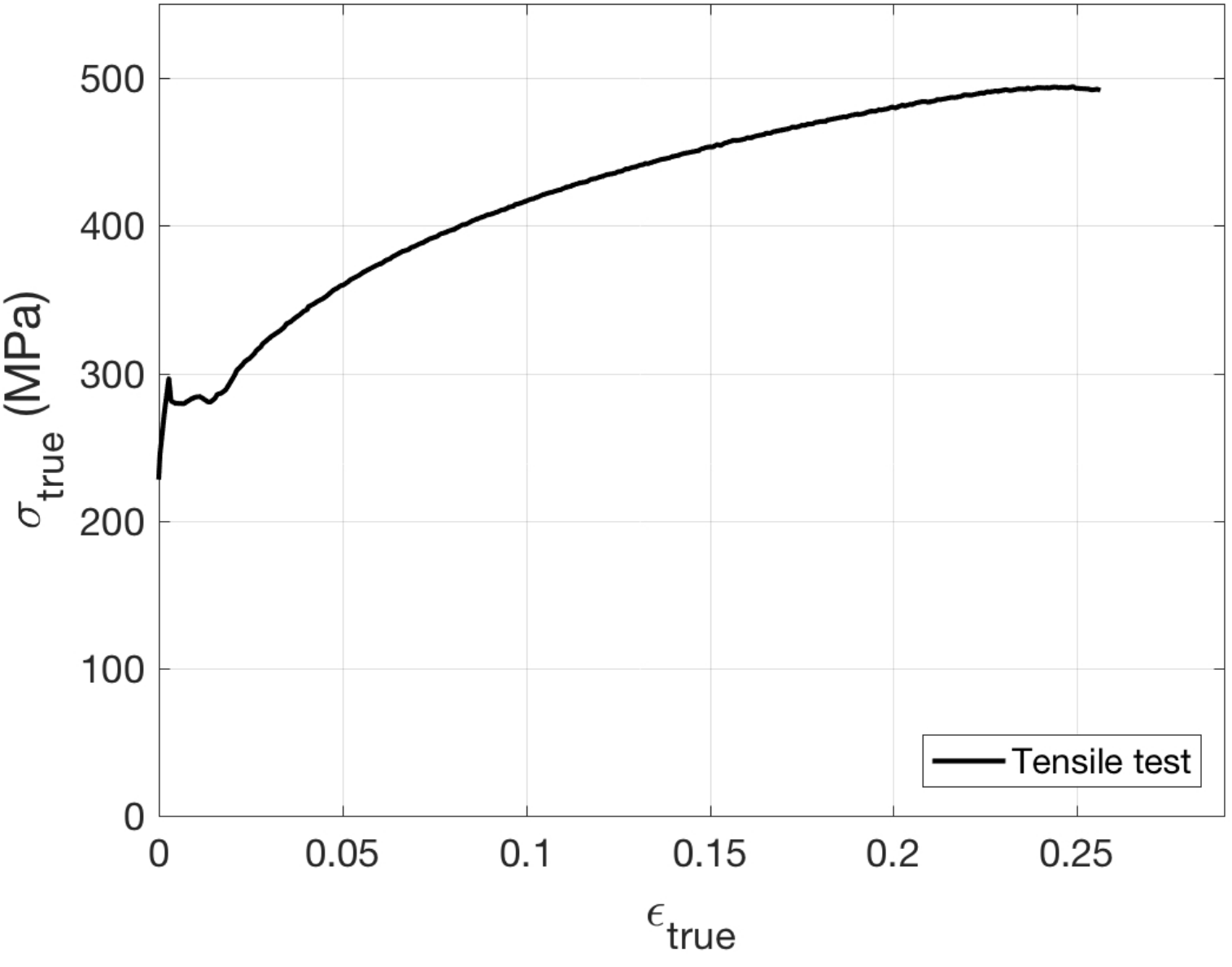
500
400
300
200
100
0
σ_{true} (MPa)
0
0.05
0.1
0.15
0.2
0.25
ϵ_{true}
Tensile test

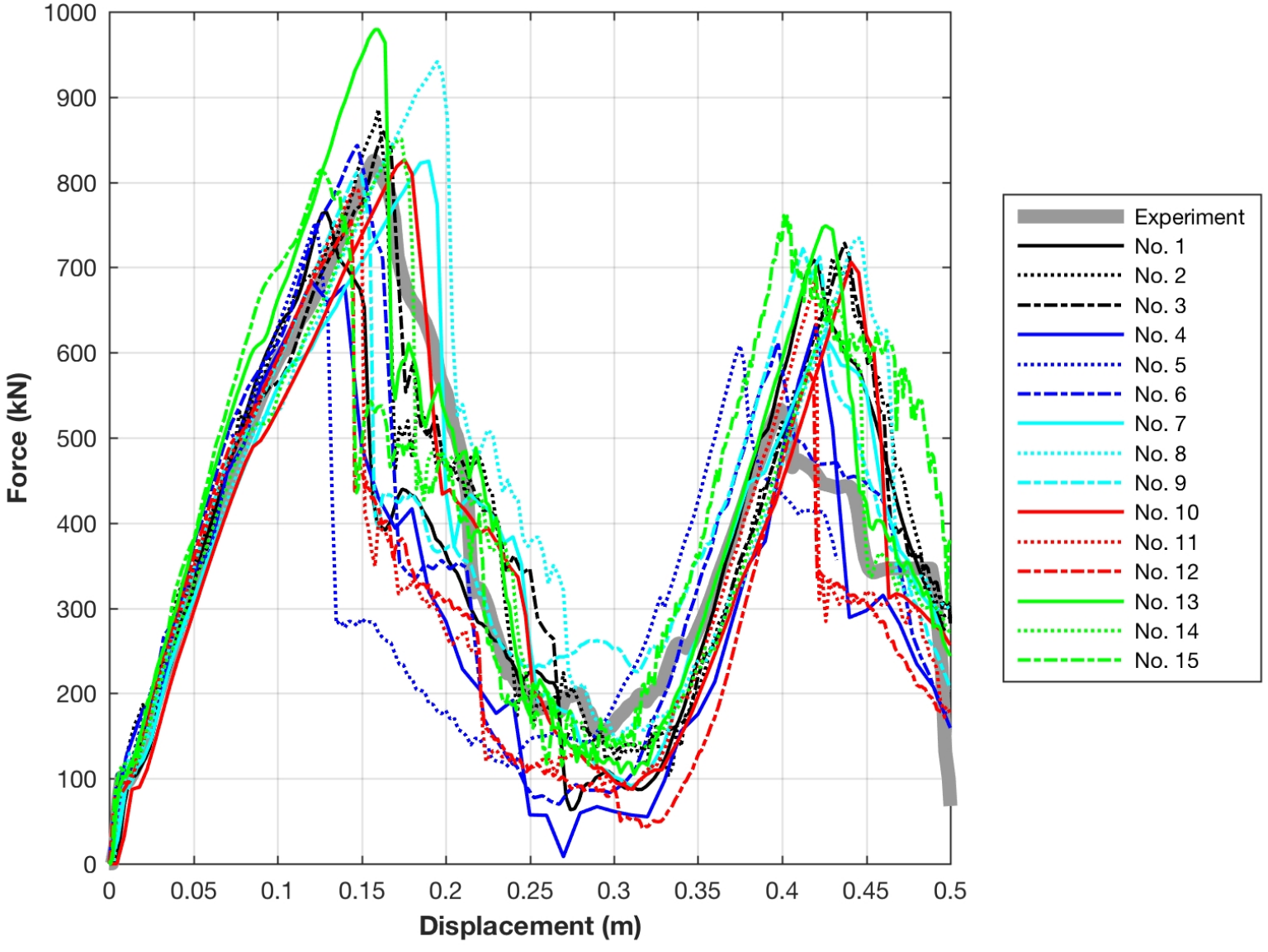
Force (kN)
Displacement (m)
0
100
200
300
400
500
600
700
800
900
1000
0
0.05
0.1
0.15
0.2
0.25
0.3
0.35
0.4
0.45
0.5
Experiment
No. 1
No. 2
No. 3
No. 4
No. 5
No. 6
No. 7
No. 8
No. 9
No. 10
No. 11
No. 12
No. 13
No. 14
No. 15

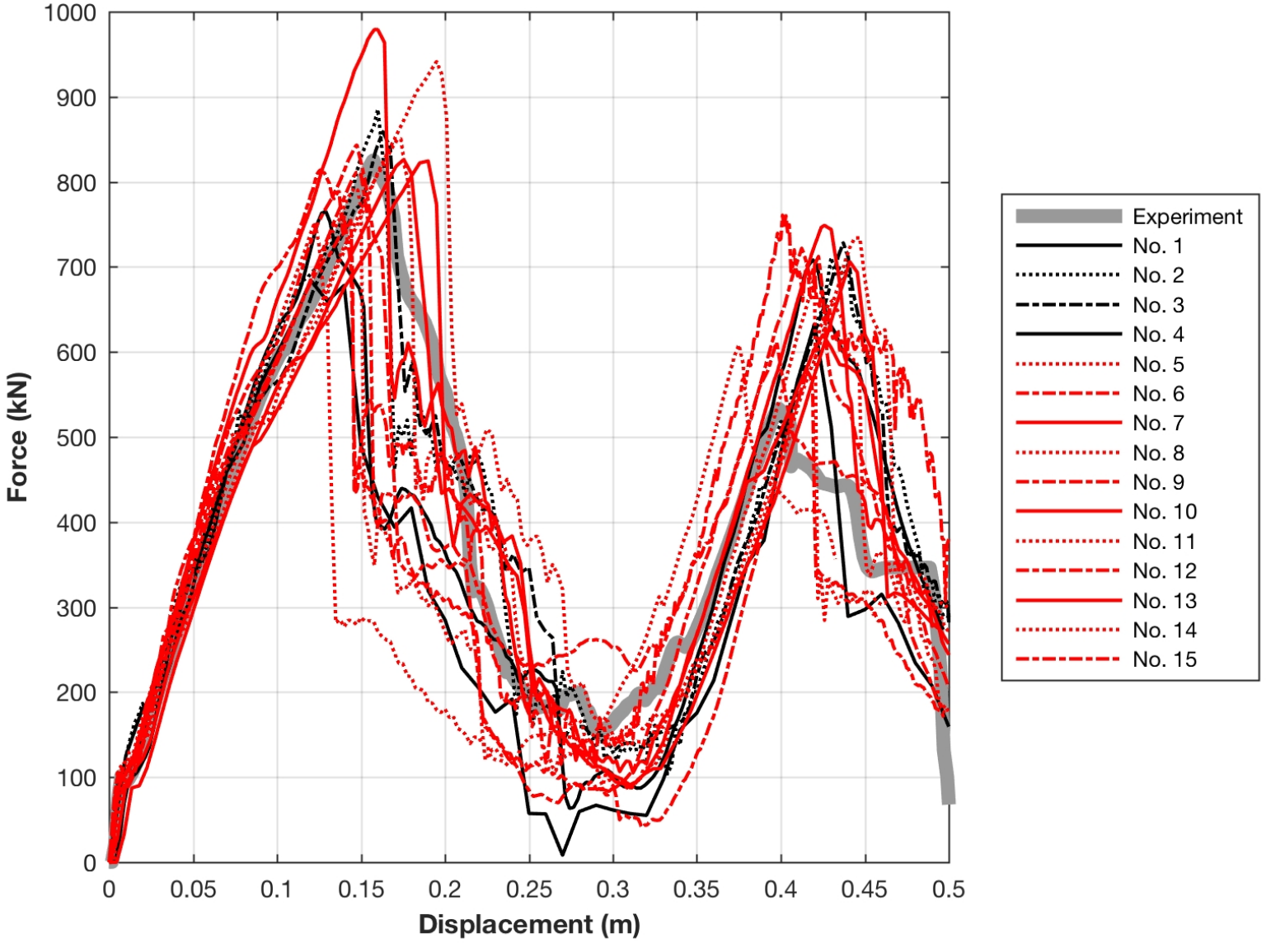
Force (kN)
Displacement (m)
0
100
200
300
400
500
600
700
800
900
1000
0
0.05
0.1
0.15
0.2
0.25
0.3
0.35
0.4
0.45
0.5
Experiment
No. 1
No. 2
No. 3
No. 4
No. 5
No. 6
No. 7
No. 8
No. 9
No. 10
No. 11
No. 12
No. 13
No. 14
No. 15

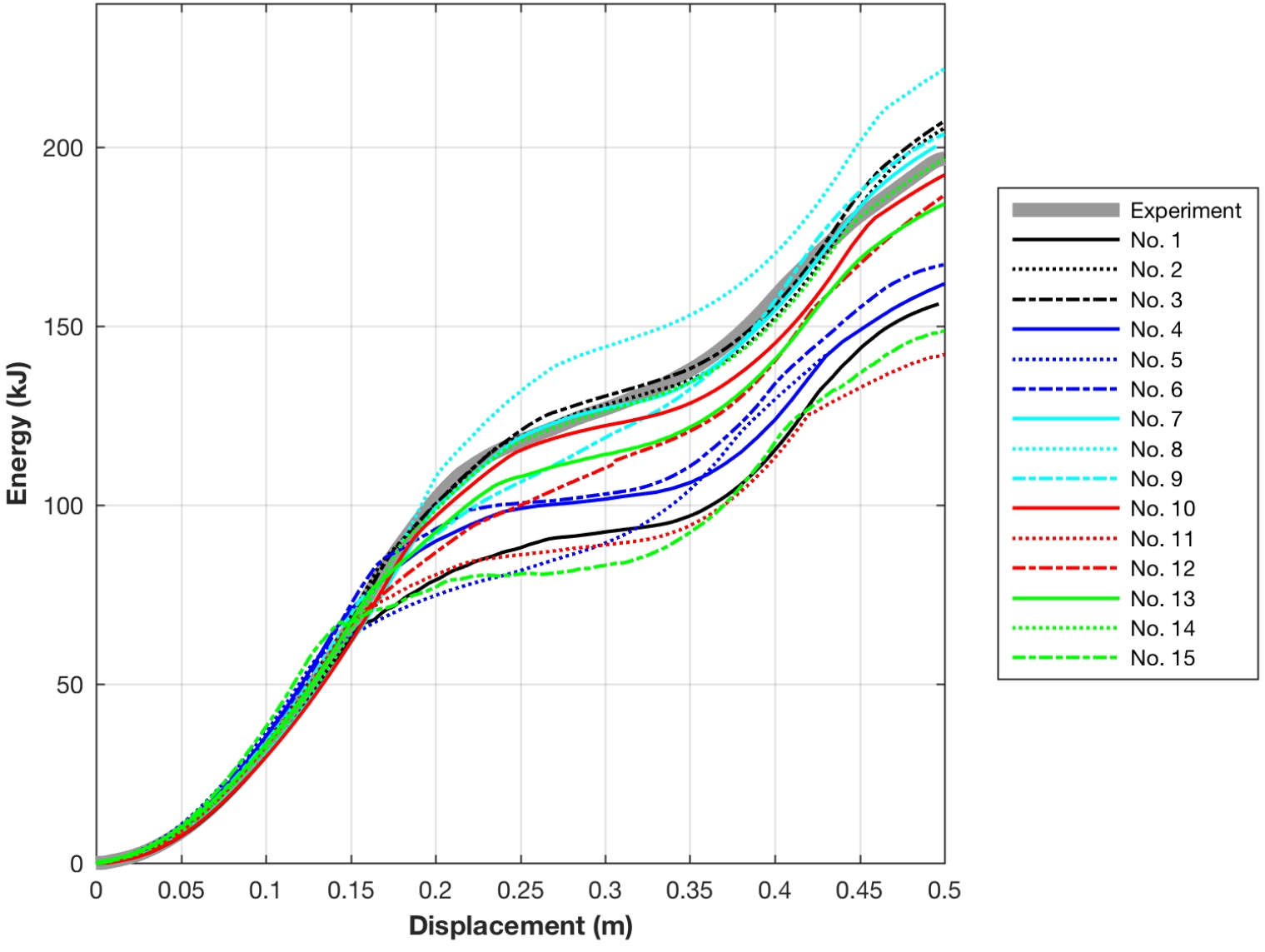
Energy (kJ)
0
50
100
150
200
0
0.05
0.1
0.15
0.2
0.25
0.3
0.35
0.4
0.45
0.5
Displacement (m)
Experiment
No. 1
No. 2
No. 3
No. 4
No. 5
No. 6
No. 7
No. 8
No. 9
No. 10
No. 11
No. 12
No. 13
No. 14
No. 15

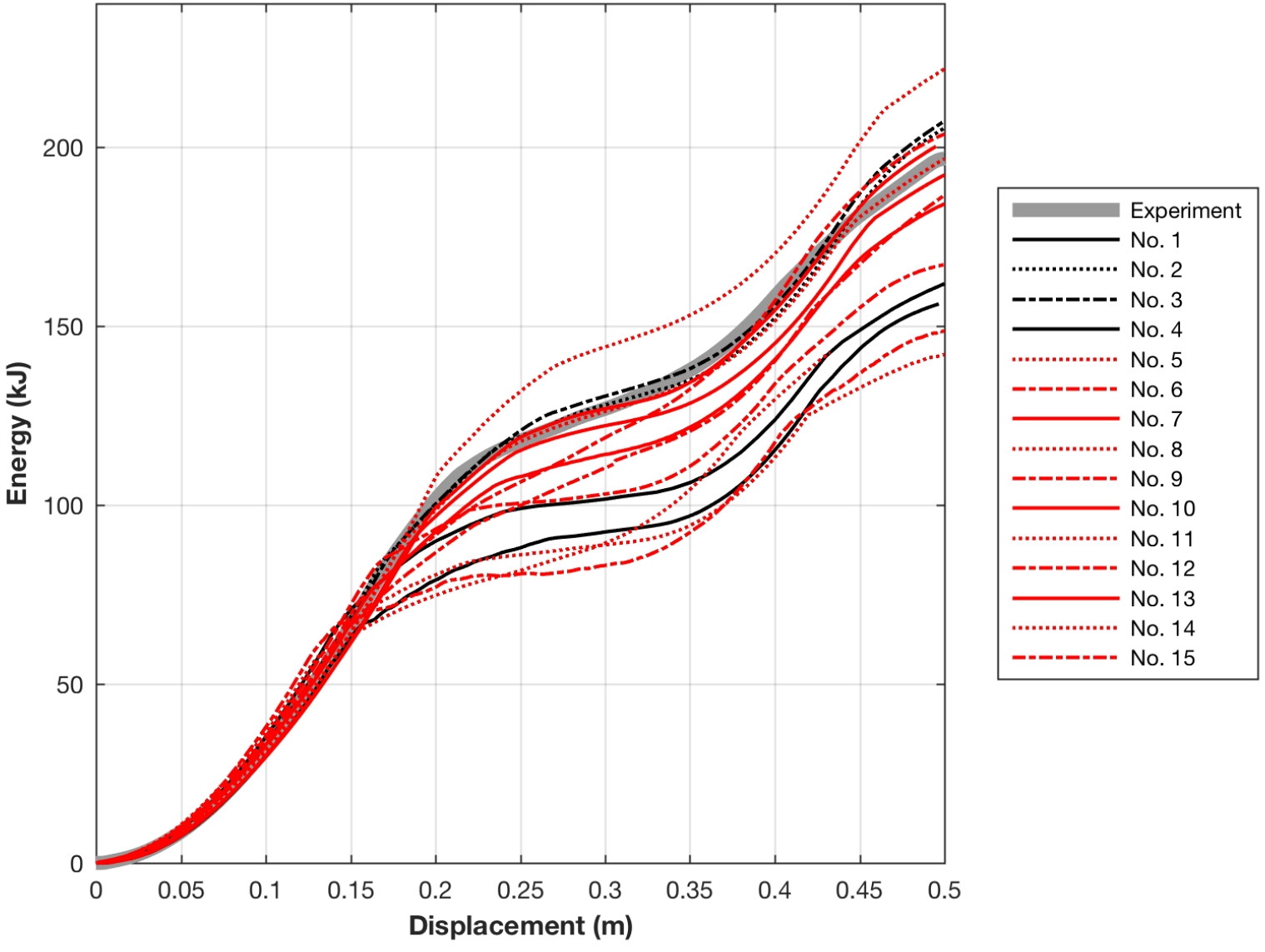
Energy (kJ)
0
50
100
150
200
0
0.05
0.1
0.15
0.2
0.25
0.3
0.35
0.4
0.45
0.5
Displacement (m)
Experiment
No. 1
No. 2
No. 3
No. 4
No. 5
No. 6
No. 7
No. 8
No. 9
No. 10
No. 11
No. 12
No. 13
No. 14
No. 15

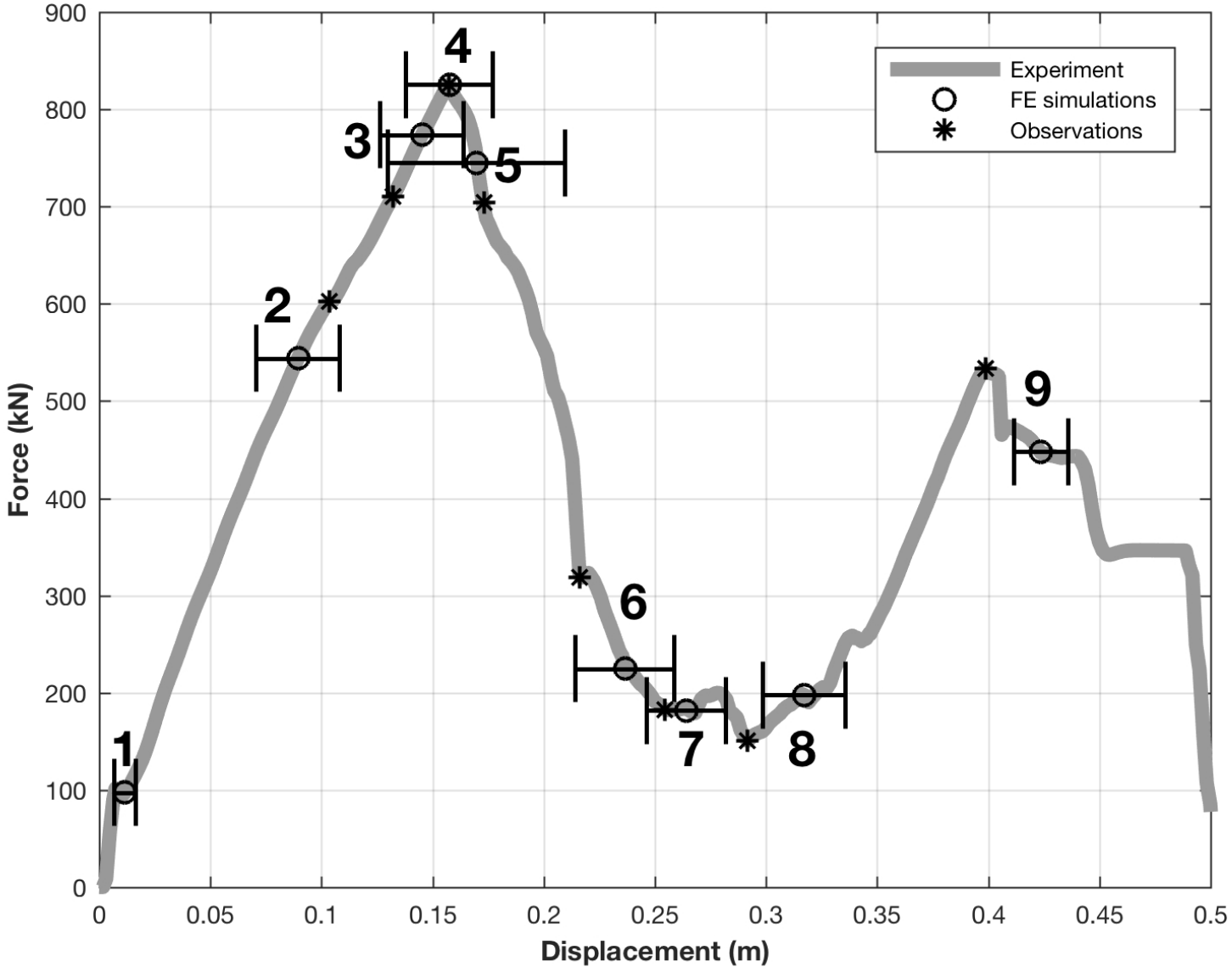
Experiment
FE simulations
Observations
Force (kN)
Displacement (m)
0
100
200
300
400
500
600
700
800
900
0
0.05
0.1
0.15
0.2
0.25
0.3
0.35
0.4
0.45
0.5
1
2
3
4
5
6
7
8
9

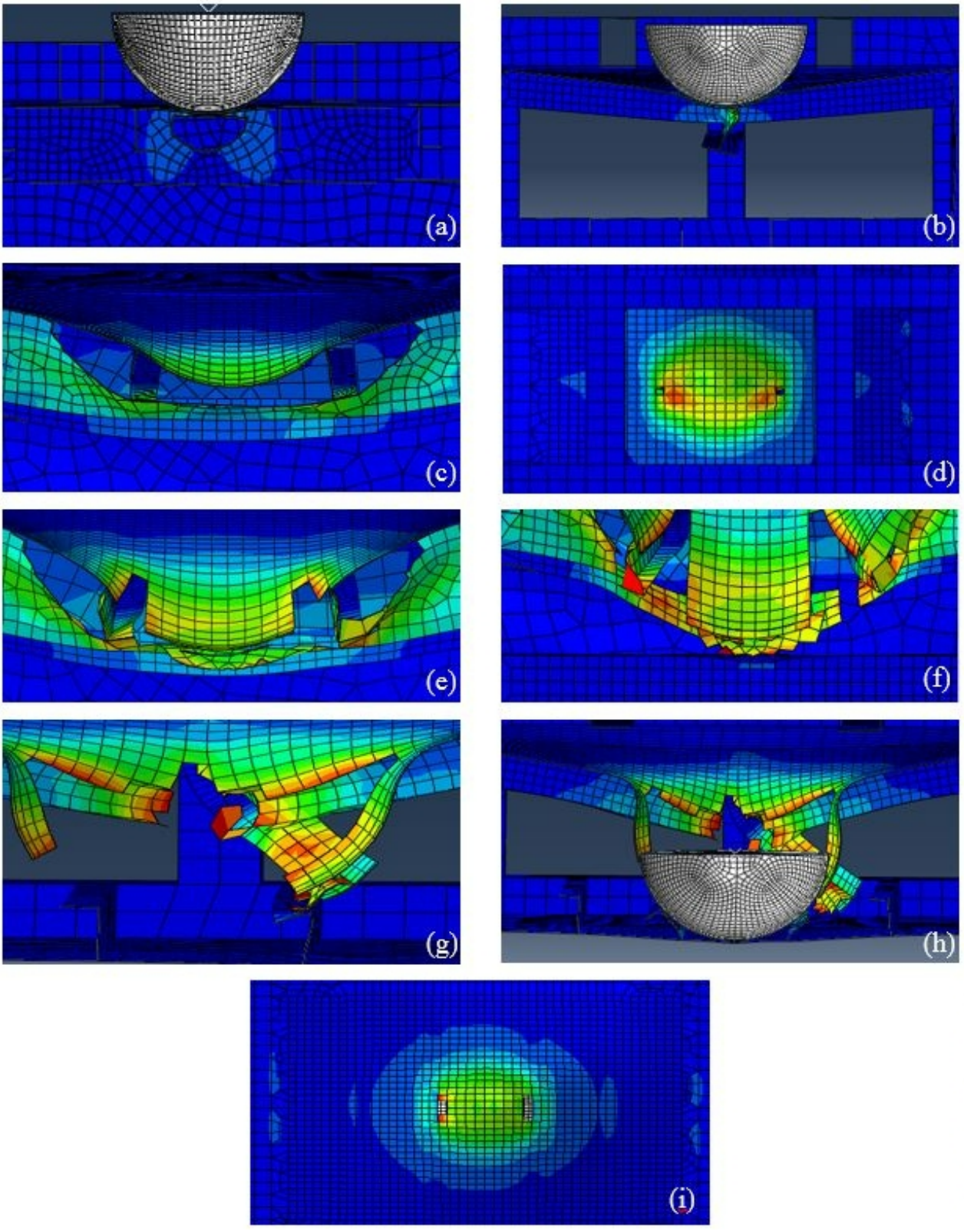
(a)
(b)
(c)
(d)
(e)
(f)
(g)
(h)
(i)

Table 1. Summary of the participants' FE model definitions and parameters.

ID	FE solver	Element type	Integration: reduced (R) or full (F)	Element size [mm]	Indenter speed [m/s]	Friction coefficient	Reinforcing frame in the model: Yes/No
1	ABAQUS/Explicit v6.13-3	S4R; hourglass control	R	Sheets: 10 Other members: 9.2-9.8	1.0	0.23	Yes
2	ABAQUS/Explicit v6.13-3	S4R; hourglass control	R	15	1.0	0.23	Yes
3	ABAQUS/Explicit v6.13-4	S4R; hourglass control	R	15	3.0	0.23	Yes
4	ABAQUS/Explicit v6.13-3	S4R; hourglass control	R	Upper sheet: 15 Lower sheet: 30	10.0	0.23	Yes
5	LS-DYNA v9.71	FE type 16	F	10	0.50	0.23	No
6	LS-DYNA v9.71, smp d R7.1.1	FE type 16	F	15	5.0	0.23	Yes
7	LS-DYNA v9.71, smp d R8.0.0	Belytschko-Lin-Tsay elements	R	10	2.0	0.23	Yes
8	LS-DYNA v9.71	Belytschko-Lin-Tsay elements	R	15	3.0	0.23	Yes
9	LS-DYNA v9.71	Hughes-Liu (HL) shell elements	R	9	0.50	0.23	Yes
10	LS-DYNA v9.71, smp d R7.0.0	Belytschko-Lin-Tsay elements	R	10	0.45	0.23	Yes
11	LS-DYNA v9.71, R7.0.0 double precision	Belytschko-Lin-Tsay elements	R	10	2.0	0.23	Yes
12	LS-DYNA v9.71, smp d R7.1.2	Belytschko-Lin-Tsay elements	R	Sheets: 10 Stiffener web: 12	0.01	0.23	Yes
13	LS-DYNA v9.71	Belytschko-Lin-Tsay elements	F	20	2.0	0.23	No
14	LS-DYNA v9.71	Belytschko-Lin-Tsay elements	R	15	2.2	0.23	Yes
15	LS-DYNA v9.71 R7.1.1	Belytschko-Lin-Tsay elements	R	10	1.0	0.23	Yes

Table 2. Constitutive material models and material parameters for the test object and the reinforcing frame.

ID	Constitutive material model	Material	Young's modulus, E [GPa]	Yield stress, σ_y [MPa]	Stress-strain relationship: curve from test or inelastic power law (K and n)	Comments
1	Isotropic hardening, inelastic Swift power law with a yield plateau [33]	NVA mild steel	206	310	K = 700 MPa n = 0.195	Own curve fit to curve from test.
2	Isotropic hardening, inelastic power law in Eq. (1)	NVA mild steel	206	290	K = 616 MPa n = 0.21	
3	Isotropic hardening, inelastic power law in Eq. (1)	NVA mild steel	206	290	K = 616 MPa n = 0.21	
4	Modified Ludwik's constitutive equation [34]	NVA mild steel	206	310.5	K = 406 MPa n = 0.468	Own curve fit to curve from test.
5	Mat.024-piecewise linear plasticity	NVA mild steel	206	290	Curve from test.	
6	Mat.024-piecewise linear plasticity	NVA mild steel	206	290	Curve from test.	
7	Mat.123-modified piecewise linear plasticity	NVA mild steel	206	325	Curve from test.	Own fit of the yield stress.
8	Mat.123-modified piecewise linear plasticity	NVA mild steel	206	290	K = 616 MPa n = 0.21	
9	Mat.024-piecewise linear plasticity	NVA mild steel	206	290	Curve from test.	
10	Isotropic hardening, inelastic power law in Eq. (1)	NVA mild steel	206	290	K = 616 MPa n = 0.21	
11	Isotropic hardening, inelastic Holloman power law with a yield plateau [35]	NVA mild steel	206	310	K = 720 MPa n = 0.21	Own curve fit to curve from test.
12	Mat.024-piecewise linear plasticity	NVA mild steel	206	310	Curve from test.	Own fit of the yield stress.
13	Mat.024-piecewise linear plasticity	K240-Z mild steel	206	235	K = 658 MPa n = 0.194	Own curve fit to curve from tests in Karlsson et al. [27].
14	Mat.024-piecewise linear plasticity	NVA mild steel	210	290	K = 616 MPa n = 0.21	
15	Mat.024-piecewise linear plasticity	NVA mild steel	206	290	Curve from test.	

Table 3. Summary of the preferred failure criterion for each FE model, how damage was modelled and values of relevant and used material parameters.

ID	Failure criterion	Clarification of the failure criterion and damage models	Necking strain, ε_n [%]	Fracture strain, ε_f [%]	Comments
1	Fracture initiation based on element size and stress state.	No separate damage evolution model after necking.	0.21	0.26	Fracture criterion as described in [36]; no damage induced softening. Calibration of fracture parameters based on tensile test.
2	Multiple damage criterion: initiation and evolution.	Damage initiation was modelled using the shear criterion; damage evolution was modelled using a bilinear damage evolution model.	0.21	0.26	See [2, 31] for details regarding the damage initiation and evolution models. Barba's law [30] is used in the FE model.
3	Shear failure criterion.	Own shear criterion in a VUMAT; see [17] for details. No separate damage evolution model after necking.		0.26	Allows for the influence of element size and thickness on the fracture strain value in the FE model according to a model in [17].
4	Shear failure criterion.	No separate damage evolution model after necking.		0.28	Allows for the influence of element size and thickness on the fracture strain value in the FE model according to a model in [37].
5	Effective plastic strain.	No separate damage evolution model after necking.		0.26	
6	Effective plastic strain.	No separate damage evolution model after necking.		0.26	
7	Effective plastic strain.	No separate damage evolution model after necking.		0.525	The fracture strain was calculated according to [38] and considered the influence of mesh size. Allows for the influence of element size on the fracture strain value in the FE model.
8	Effective plastic strain.	No separate damage evolution model after necking.		0.45	The fracture strain was calculated according to a model in [15]. Allows for the influence of element size and thickness on the fracture strain value in the FE model.
9	Effective plastic strain.	No separate damage evolution model after necking.		0.35	The value of the fracture strain was revised using Barba's law [30] to match the mesh size of the FE model.
10	Effective plastic strain.	No separate damage evolution model after necking.		0.43	The value of the fracture strain was studied in a parametric study (mesh size was one of the parameters) before one

					recommended and final value was decided.
11	The BWH (Bressan-Williams-Hill) instability criterion in [39].	The criterion was used without the post-necking damage model presented in [21].	0.21		The fracture strain is not used in the failure criterion.
12	The Germanischer Lloyd (GL) criterion based on thru thickness plastic strain [1].	No separate damage evolution model after necking.		0.26	
13	Effective plastic strain.	No separate damage evolution model after necking.		0.35	The value of the fracture strain was studied in a parametric study (mesh size was one of the parameters) before one recommended and final value was decided.
14	Effective plastic strain.	No separate damage evolution model after necking.		0.39	The value of the fracture strain was studied in a parametric study (mesh size was one of the parameters) before one recommended and final value was decided.
15	Effective plastic strain.	No separate damage evolution model after necking.		0.315	Barba's law [30] is used in the FE model.

Table 4. Summary of the preferred failure criterion for each FE model, how damage was modelled and values of relevant and used material parameters.

Event No.	Description of the event	Experiment: indenter displacement [mm]	FE simulations: mean value of the indenter displacement [mm]	FE simulations: standard deviation of the indenter displacement [mm]	No. of participants that identified the event in their FE simulation
1	Initiation of plasticity expansion of the T-beam.	No data available.	11.6	4.7	15
2	Tripping of the T-beam.	103	89.4	18.9	14
3	Buckling of the webs of the two central L-profiles attached to the upper sheet.	132	145.2	18.8	11
4	Fracture initiation of the upper sheet.	157	157.6	19.6	15
5	Folding of the webs of the two central L-profiles attached to the upper sheet.	173	169.7	39.7	14
6	T-beam off.	216	236.6	22.3	13
7	T-beam starts to contact with the L-profile attached to the lower sheet.	254	264.2	17.8	14
8	Contact of the striker with the lower sheet.	291	317.2	18.7	15
9	Fracture initiation of the lower sheet.	399	423.6	12.2	15